Temperature and pH Dependences of Hydrogen Exchange and Global Stability for Ovomucoid Third Domain†

Liskin Swint-Kruse‡ and Andrew D. Robertson*

Department of Biochemistry, The University of Iowa, Iowa City, Iowa 52242

Received July 31, 1995; Revised Manuscript Received October 30, 1995⊗

ABSTRACT: Two-dimensional nuclear magnetic resonance spectroscopy has been used to monitor proton−deuterium exchange rates (k_{obs}) for more than 30 residues in turkey ovomucoid third domain. To test whether exchange is governed by global unfolding, rates were measured over a wide range of pH and temperatures where the change in the free energy of unfolding (ΔG°_u) is known [Swint, L., & Robertson, A. D. (1993) *Protein Sci. 2*, 2037−2049; Swint-Kruse, L., & Robertson, A. D. (1995) *Biochemistry 34*, 4724−4732]. Under conditions where EX2 kinetics are observed, a subset of 6−11 residues exhibits a one-to-one correlation with global stability. These residues are all located in central regions of secondary structures. Many other sites show varied degrees of correlation with ΔG°_u, while some are slower than expected on the basis of ΔG°_u alone. Preliminary evidence suggests that the latter is due to deviation from EX2 kinetics, even though experimental conditions are relatively mild (pH* 3 and 40 °C) compared to those in which deviations were observed for bovine pancreatic trypsin inhibitor. These results, together with similar observations for hen egg white lysozyme and barnase, suggest that EX2 kinetics should not be assumed when interpreting exchange studies.

Hydrogen exchange of amide backbone protons is utilized to identify stabilizing interactions, folding intermediates silent in other experiments, and ligand binding sites in proteins (Woodward & Hilton, 1979; Roder, 1989; Scholtz & Robertson, 1995). Exchange rates are slowed relative to those of unstructured peptides and have long been postulated to be affected by surrounding structure (Linderstrøm-Lang, 1955). The mechanism by which protein structure slows exchange has been much debated (Hvidt & Nielsen, 1966; Wagner & Wüthrich, 1979; Woodward & Hilton, 1980; Barksdale & Rosenberg, 1982; Englander & Kallenbach, 1984). Models to explain slow exchange have ranged from cooperative structural fluctuations with concomitant exposure of the exchange site (Hvidt, 1964; Englander et al., 1980; Wüthrich et al., 1980) to solvent penetration through noncooperative fluctuations (Woodward & Hilton, 1980). Nevertheless, several proponents of the various models have agreed upon a two-process model for exchange (Rosenberg & Chakravarti, 1968; Woodward & Hilton, 1980; Bai et al., 1994; Qian et al., 1994).

According to the two-process model, exchange occurs via two competing pathways: (1) global unfolding followed by exchange from unstructured protein and (2) exchange from native protein. Often, the slowest exchanging sites in a protein are assumed to exchange solely by the first pathway; their exchange rates have been interpreted as measures of the unfolding equilibrium constant (K_u),[1] and therefore ΔG°_u (Roder, 1989; Jandu et al., 1990; Clarke et al., 1993; Kim et al., 1993; Loh et al., 1993; Mayo & Baldwin, 1993; Bai et al., 1994; Perrett et al., 1995). If exchange from a subset of sites is indeed dominated by pathway 1, then these sites present an opportunity for testing elements of the two-process model (Perrett et al., 1995).

The use of hydrogen exchange experiments to analyze protein stability is based upon three rarely tested assumptions. First, the slowest exchange is dominated by global unfolding (pathway 1). Second, the rate of protein refolding is faster than exchange from the exposed site (EX2 kinetics; Hvidt, 1964). Third, no interactions remain in unfolded protein to further slow exchange. When these criteria are met, K_u and ΔG°_u may be calculated from the observed exchange rate (k_{obs}) and that predicted from unstructured peptides (k_{int}):

$$K_u = \frac{k_{obs}}{k_{int}} \quad (1)$$

and

† This work was supported by a grant from the National Institutes of Health (GM 46869). L.S.K. is an Iowa Fellow at The University of Iowa.

* FAX: (319) 335-9570. E-mail: andy-robertson@uiowa.edu.

‡ Present address: Department of Biochemistry and Cell Biology, Weiss School of Natural Sciences, Rice University, Houston, TX 77251.

⊗ Abstract published in *Advance ACS Abstracts,* December 15, 1995.

[1] Abbreviations: ΔG°_u, the change in Gibbs free energy for protein unfolding; D_2O, deuterium oxide; NMR, nuclear magnetic resonance; HEW lysozyme, hen egg white lysozyme; K_u, equilibrium constant of unfolding; k_{int}, calculated intrinsic exchange rate; k_{obs}, observed exchange rate; OMTKY3, turkey ovomucoid third domain; NOE, nuclear Overhauser effect; pK_a, acid dissociation constant; υ, the normalized volume of an amide proton cross-peak; a, amplitude of an exchange decay curve; t, time in hours; c, a constant value describing the offset of the exchange curve from zero; K_1, equilibrium constant describing interconversion of native protein states; k_1, rate of protein unfolding or other "opening" event; k_2, rate of protein folding or other "closing" event; pH_{min}, the pH at which hydrogen exchange is slowest; k_{min}, the exchange rate at pH_{min}; EX1, mechanism of hydrogen exhange in which k_{obs} is equal to k_1; EX2, mechanism of hydrogen exchange in which k_{obs} is equal to k_1/k_2k_{int}; P_A and P_B, the probabilities that sites A and B are protonated, respectively; k_A and k_B, the hydrogen exchange rates for sites A and B; P_{AB}, the probability that an NOE exists between sites A and B; k_{AB}, the rate of disappearance of NOE AB; BPTI, bovine pancreatic trypsin inhibitor; RNase A, ribonuclease A.

0006-2960/96/0435-171$12.00/0

$$\Delta G_u^\circ(\text{hydrogen exchange}) = -RT \ln (K_u) = -RT \ln\left(\frac{k_{obs}}{k_{int}}\right) \quad (2)$$

Values of k_{int} are calculated for any amino acid sequence according to the procedures of Molday et al. (1972) and Bai et al. (1993). These predicted rates generally agree well with those measured in denatured proteins (Roder et al., 1985b; Robertson & Baldwin, 1991; Lu & Dahlquist, 1992; Radford et al., 1992; Arcus et al., 1994; Buck et al., 1994). For clarity, all hydrogen exchange results in this manuscript are reported as $-RT \ln(k_{obs}/k_{int})$; values labeled "ΔG_u°" are not calculated from eq 2 but are determined from independent thermal denaturation experiments (Swint-Kruse & Robertson, 1995).

Several studies have focused on correlations between free energies of stabilization and hydrogen exchange. In many cases, ΔG_u° and the exchange rates have not been measured independently under the same solution conditions (Kim & Woodward, 1993; Mayo & Baldwin, 1993; Bai et al., 1994). Roder concluded that his efforts with BPTI (1989) were limited by uncertainties in values of k_{int} in mixed solvents. Some of the most informative studies have been performed with helical peptides (Shalongo et al., 1994; Rohl & Baldwin, 1994), the six tryptophan side chains of hen egg white lysozyme (HEW lysozyme) (Wedin et al., 1982) and the backbone amide protons of barnase (Perrett et al., 1995). Shalongo et al. (1994) demonstrated that, for individual amide protons, the degree of protection from hydrogen exchange is in good agreement with the fractional helicity of corresponding carbonyl hydrogen bond acceptors, determined with ^{13}C-NMR spectroscopy. Rohl and Baldwin (1994) showed quantitative agreement between slow exchange and a well-established statistical mechanical treatment of hydrogen bonding in helical peptides. The work on HEW lysozyme provided good evidence for exchange limited by global unfolding (Wedin et al., 1982). Very recent results for barnase demonstrate good agreement between stability measured by hydrogen exchange and calorimetry (Perrett et al., 1995). In this manuscript, we present a rigorous test of the relationship between amide proton exchange and ΔG_u° in turkey ovomucoid third domain (OMTKY3), utilizing a wide range of experimental conditions. In addition, the assumption of EX2 kinetics has been tested by examining the cooperativity of exchange between neighboring amides using two-dimensional nuclear Overhauser enhancement spectroscopy (NOESY; Wagner, 1980).

The best way to identify the residues whose exchange is dominated by global unfolding is by comparing hydrogen exchange with results of denaturation experiments. These correlation experiments must be performed under carefully matched solution conditions, since pH, D_2O, varied protein concentration, and varied ionic strength may affect protein stability (Hermans & Scheraga, 1959; Jencks, 1969; Lemm & Wenzel, 1981; Horovitz et al., 1990; Stigter & Dill, 1990; Šali et al., 1991; Connelly et al., 1993; Swint & Robertson, 1993; Antosiewicz et al., 1994; Swint-Kruse & Robertson, 1995). We have monitored hydrogen exchange for OMTKY3 under conditions identical to those of thermal denaturation experiments used to determine ΔG_u° (Swint & Robertson, 1993; Swint-Kruse & Robertson, 1995). Exchange experiments have been conducted at 30 °C over the pH range of 1.4−5.0 and at pH 5.0 at temperatures ranging from 27 to 55 °C. To identify those residues that exchange only when OMTKY3 unfolds, correlation plots have been constructed to determine which values of $-RT \ln(k_{obs}/k_{int})$ (eq 2) are equal to ΔG_u° determined from independent thermal denaturation experiments (Swint-Kruse & Robertson, 1995).

MATERIALS AND METHODS

Domestic turkey (*Maleagris gallopavo*) eggs were a gift from Theis Farms (New Haven, IA); purification of OMTKY3 was performed as described by Swint and Robertson (1993). Deuterium oxide (99.9 atom %, D_2O) and sodium deuteroxide were obtained from Cambridge Isotope Laboratories (Cambridge, MA), and deuterium chloride was purchased from Stohler Isotope Chemicals (Rutherford, NJ). Exchange buffer consisted of 10 mM potassium acetate and 10 mM potassium phosphate in D_2O; the latter had been previously lyophilized from D_2O to minimize the proton concentration in the buffer. The pH of all samples was measured at the beginning and end of each experiment using an Orion Research model 611 pH meter equipped with a 3 mm Ingold electrode (Wilmad Glass Company, Buena, NJ) calibrated at two points with standards from VWR Scientific (West Chester, PA) and Fisher Scientific (Pittsburgh, PA). The estimated uncertainty in pH measurements is 0.04 pH units. Values of pH* reported for D_2O solutions represent apparent pH values, without correction for isotope effects.

NMR data were acquired on a Varian UNITY spectrometer, located in the College of Medicine at the University of Iowa, operating at 500 MHz proton frequency and equipped with an ID500-5 probe from Nalorac Cryogenics Corporation (Martinez, CA). Prior to sample preparation, the spectrometer's variable temperature controller was calibrated using a methanol standard (Van Geet, 1968). The uncertainty in these calibrations and in the stability of the temperature controller is ±0.5 °C. For each sample, the temperature was calibrated immediately prior to data acquisition. Shims were also preadjusted on a sample similar to the exchange sample.

Exchange samples were prepared by lyophilizing aliquots from a stock solution of OMTKY3. The aliquot volume was chosen so that the final protein concentration was 2 mM when redissolved in 800 μL of cold buffer. The pH* of the sample was quickly adjusted, and the sample was filtered through a Millipore Millex-GV 0.22 μm filter unit. A 700 μL aliquot was then transferred to a 5 mm NMR tube. If exchange was to be monitored below 35 °C, the sample was kept on ice during the preceding manipulations. After transferring the sample tube to the spectrometer, the lock signal was monitored in order to determine when the sample temperature had equilibrated with that of the spectrometer, the shims were readjusted, and data acquisition was begun. Equilibration and adjustment usually took 15−20 min. Both 1D and 2D spectra were acquired at 20−30 time points for most experiments. The sample was kept at the appropriate temperature in a water bath during long intervals between time points.

For exchange at pH* 5.0, 48 and 55 °C, the sample was incubated in a water bath at the appropriate temperature for the desired time interval, exchange was quenched by cooling

in ice water (Wagner & Wüthrich, 1982), and spectra were acquired at 27 °C. The same sample was then returned to the bath for the next time point. Sample temperature reached 48 °C in less than 20 s and 55 °C in approximately 30 s. Since OMTKY3 amide proton exchange at 27 °C is generally 2 orders of magnitude slower than that at 48 °C, exchange during data collection was minimal. Furthermore, since the time elapsed during acquisition at 27 °C was about the same for each time point, the observed rate constant is a function of exchange at only the higher temperature (Wagner & Wüthrich, 1982; Wang et al., 1995). The same argument holds for the time elapsed while raising the temperature of the sample from 27 °C to the exchange temperature.

During data acquisition, the carrier frequency of the NMR spectrometer was set on the water signal and the spectral width was typically 6000 Hz. Two to four steady state pulses were applied at the beginning of each experiment. The relaxation delay was 1.5 s. 1D data sets were the sum of 16 transients; each had 8000 time-domain data points. These experiments took 1 min to complete. Prior to Fourier transformation, 1D data were zero-filled to 8192 data points. COSY spectra (Aue et al., 1976) consisted of 256 blocks of four summed transients; each transient had 1024 time-domain points. Total acquisition time was 33 min.

COSY experiments were processed using the NMRI option of SYBYL (Versions 6.0 and 6.1, Tripos Associates, Inc., St. Louis, MO) installed on a Silicon Graphics 4D-35 Personal Iris workstation. Data were apodized in each dimension with an unshifted sine bell prior to Fourier transformation. The water signal was set at 4.76 ppm and used as the chemical shift standard. The cross-peaks of $C_\alpha H$/NH were identified according to the assignments of Robertson et al. (1988). Proton occupancies were determined using the integration utility of NMRI. An attempt was made to compensate for base plane differences between spectra by subtracting volumes obtained in regions of noise from cross-peak volumes, but this only diminished data quality. Therefore, base plane differences have been neglected in rate determinations. Peak volumes were normalized to the sum of the volumes of three nonexchangeable peaks: the $C_\beta H/C_\gamma H$ cross-peak from Val 41, the $C_\delta H/C_\epsilon H$ cross-peak of Tyr 20, and either the $C_\beta H/C_{\beta'} H$ cross-peak of His 52 or the $C_\gamma H/C_\delta H$ cross-peak of Leu 50. Normalized volumes of nonexchanging standard peaks usually deviated less than 5% over the course of the exchange experiment.

Hydrogen exchange rates were determined by fitting normalized peak volume versus time to the equation

$$v = a \exp(-k_{obs} t) + c \qquad (3)$$

where v represents the normalized volume of the cross-peak, a represents the amplitude of the exchange curve, k_{obs} is the rate of hydrogen exchange, t is the time in hours, and c is a constant. Nonlinear regression was performed using a version of NonLin (Johnson & Frasier, 1985; Johnson & Faunt, 1992) modified to run on Apple Macintosh computers by Robert Brenstein (Robelko Software, Carbondale, IL). Rate constants were only determined for sites for which at least three data points were obtained. In the event of overlapping peaks, the two rate constants could sometimes be determined by fitting the data to the sum of two exponentials (Tüchsen & Woodward, 1985a). Values of k_{int} for each exchangeable amide proton at all temperatures and pH* were calculated according to Bai et al. (1993). Ionization states of acidic groups, determined from their respective pK_as (Schaller & Robertson, 1995), were included in these calculations.

Solvent accessible surface areas were calculated using the crystal structure of silver pheasant third domain (Bode et al., 1985), which differs from OMTKY3 by only one solvent-exposed residue (Laskowski et al., 1987). These calculations were performed with the Lee and Richards algorithm (1971) as implemented in the program Access by Scott Presnell (UCSF). Solvent probe radius was 1.4 Å.

For EX1 versus EX2 tests at pH* 3.0, 40 °C, exchange was monitored in real-time with NOESY spectra (Kumar et al., 1980) collected at 40 °C. The number of time points that could be obtained from one sample was limited to less than 8 by the 6 h acquisition time. Therefore, additional time points were obtained from a second sample that was incubated at 40 °C for 1.5 h prior to data collection at 40 °C. Handling differences resulted in different amplitudes and signal-to-noise in the data of the two samples. Therefore, the data were simultaneously fit with eq 3 as two separate peaks monitoring the same event, with a common value of k_{obs} and separate values of a and c.

NOESY data were processed using the NMRI option of SYBYL. Data were apodized in both dimensions with a Gaussian function using line broadening of 8 and 30 Hz in the t2 and t1 dimensions, respectively. Data in the $t1$ dimension were zero-filled once prior to Fourier transformation. The water signal was set at 4.76 ppm and used as the chemical shift standard. The cross-peaks for NH/NH and CH/NH NOEs were identified according to the assignments of Robertson et al. (1988). Proton occupancies were determined using the integration utility of NMRI and normalized to the volumes of nonexchanging peaks, such as the $C_\alpha H/C_\gamma H$ of Val 41, the $C_\beta H/C_\gamma H$ of Leu 50, and the $C_\alpha H/C_\beta H$ of Tyr 20. All normalized intensities were fitted with eq 3. In cases where more than one CH/NH cross-peak could be distinguished for the same residue, the data were simultaneously fitted with a common value of k_{obs} and separate values of a and c.

RESULTS

Exchange rates for OMTKY3 have been measured over a wide range of pH* and temperature where ΔG_u° is known with confidence from independent thermal denaturation experiments (Swint-Kruse & Robertson, 1995). Buffer and solvent (D_2O) are identical in the studies of hydrogen exchange and global stability, and the thermodynamics of unfolding are independent of protein concentration (Swint & Robertson, 1993). We are thus able to test the assumption that the most slowly exchanging sites are controlled predominantly by the global unfolding pathway. Exchange reactions have been monitored with 2D ^{1}H NMR experiments. Typical fingerprint regions, which contain $C_\alpha H$/NH cross-peaks, of COSY spectra obtained during the course of an experiment are presented in Figure 1. Cross-peaks for more than 30 of the 52 possible residues are well resolved at time zero. The rate of disappearance after dissolution in D_2O was on the order of hours for most peaks, but some reactions at pH* > 3 were monitored for up to 6 months. The decay rates for nearly all peaks observed in the spectrum at time zero could be determined in at least a subset of the pH* and temperature experiments.

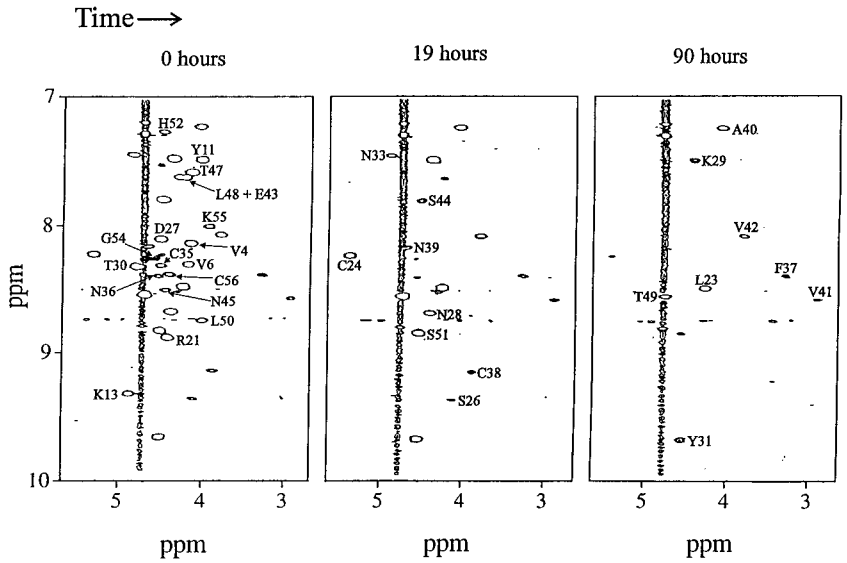

FIGURE 1: Fingerprint regions of COSY spectra for OMTKY3. OMTKY3 was dissolved in D_2O, pH* 2.5 with exchange buffer, and monitored as a function of time at 30 °C. The diminishing volumes of cross-peaks were used to quantitate proton−deuterium exchange at backbone amides.

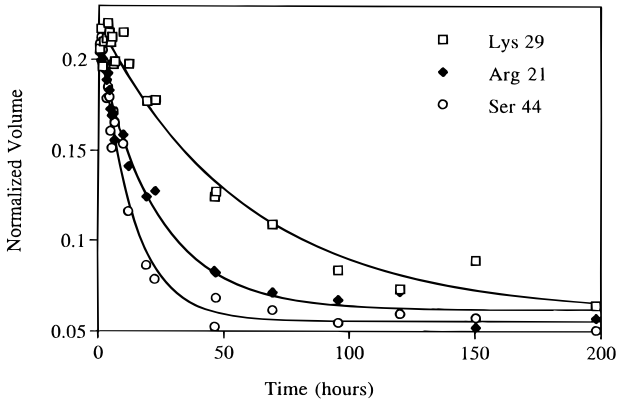

FIGURE 2: Hydrogen exchange for Lys 29 (□), Arg 21 (◆), and Ser 44 (○). Exchange was monitored at pH* 2.5, 30 °C. Decay curves were generated from $C_\alpha H$/NH cross-peaks normalized to nonexchanging peaks and fit with eq 3 (solid lines).

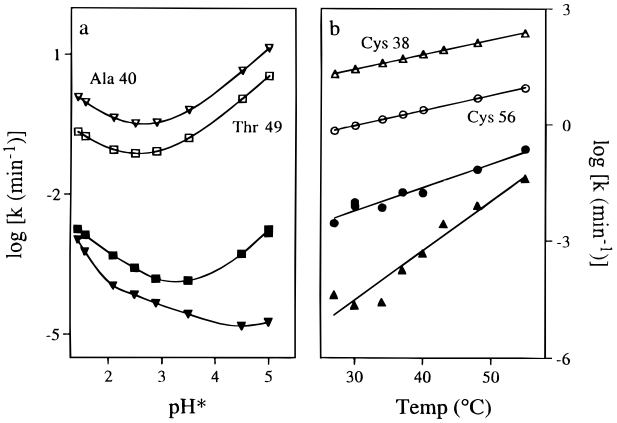

FIGURE 3: Observed versus predicted exchange rates. Observed exchange rates (k_{obs}) determined from eq 3 are plotted as functions of pH* (Thr 49, ■; Ala 40, ▼) and temperature (Cys 38, ▲; Cys 56, ●) and compared to rates predicted for unstructured peptides (Bai et al., 1993; k_{int}; □, ▽, △, ○). The solid lines are visual aids only and do not represent fitted parameters.

Most peaks not observed in the initial spectra are from surface residues, which exchange too fast to measure with these techniques. To observe a cross-peak, we estimate that the rate of exchange must be ≤ 0.03 min^{-1}, the reciprocal of the dead time for the experiment. Calculated rates at pH* 2.5 and 30 °C, where intrinsic rates are generally slowest, range from 0.06 to 0.78 min^{-1}, so upper limits for protection at these sites are 2−25-fold. As intrinsic rates increase with changes in pH* and increasing temperature, the limit of detectable slowing also increases. One residue not observed in the present study is Gly 25. Although Gly 25 exchange is known to be slow (Robertson, 1988; Robertson et al., 1988), its cross-peaks were too weak to measure in these COSY experiments.

First-order decay curves derived from hydrogen exchange experiments are presented in Figure 2. Observed rate constants (k_{obs}) were determined by fitting the data with eq 3 and are available as supporting information. Errors of the fit for k_{obs} vary widely, but repeated experiments at pH* 3.5 and 5.0 are in good agreement. In Figure 3, k_{obs} is compared to the intrinsic rate of exchange predicted for unstructured peptides (k_{int}; Bai et al., 1993) as a function of (a) pH* and (b) temperature. The observed exchange rates from the protein are slower than the intrinsic rate for all sites but valines 4 and 6 (data not shown), which have very slow intrinsic rates, 0.04 and 0.05 min^{-1}, respectively, at pH* 2.5 and 30 °C.

Values of k_{int} for amides of acidic ionizing residues, as well as residues C-terminal to these amino acids, are affected by the charged state of the side chain. Carboxyl pK_as are known for native OMTKY3 (Schaller & Robertson, 1995): for Asp 27, Glu 43, and Cys 56 they are <2.3, 4.7, and 2.4, respectively. However, if exchange is occurring from denatured OMTKY3, the pK_as for denatured protein might be more appropriate. The pK_as for Glu 43 and Cys 56 are not much different than model compound values (Schaller & Robertson, 1995; Swint-Kruse & Robertson, 1995), and the differences have little effect on calculated values of k_{int} (see Discussion). However, the pK_a for Asp 27 in denatured OMTKY3 is probably much larger than in native protein. The consequences of this difference are considered in the Discussion.

Slowed exchange in proteins has been attributed to a variety of structural features. In OMTKY3, all protected

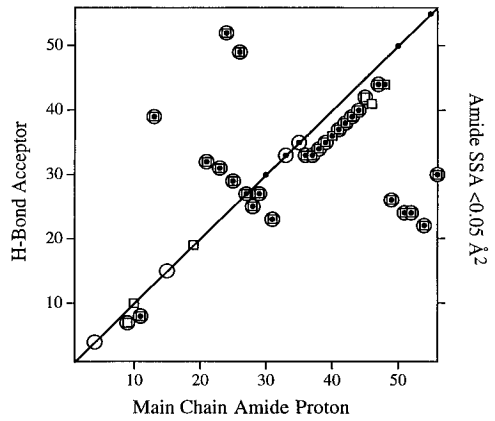

FIGURE 4: Examination of the structural basis for slowed hydrogen exchange (●). The axes represent the 56 amino acid residues in OMTKY3. (□) Hydrogen bond exists between the amide backbone proton and either a main chain or side chain residue. (○) Solvent-exposed surface area (SSA) for the amide backbone proton is <0.05 Å^2.

amide protons except Thr 30, Asn 33, Cys 35, Leu 50, and Lys 55 are involved in hydrogen bonds (Fujinaga et al., 1987; Krezel et al., 1994; Schaller & Robertson, 1995; Figure 4, ⊡). Furthermore, all sites but Thr 30, Ala 40, Leu 50, and Lys 55 have little solvent-exposed surface area (Lee & Richards, 1971; Figure 4, ⊙). Most sites involved in hydrogen bonds or excluded from solvent show protected exchange; those that do not (Figure 4, □ and ○) are in regions of irregular structure (Fujinaga et al., 1987; Krezel et al., 1994).

Numerically, exchange protection is often expressed as the quantity $(k_{obs}/k_{int})^{-1}$. If this quantity does indeed represent an equilibrium constant (eq 1), then $-RT \ln(k_{obs}/k_{int})$ is comparable to a free energy and, when plotted against values of ΔG_u° determined from independent thermal denaturation experiments, may serve as a diagnostic tool for interpreting exchange results (Roder, 1989). Sites that exchange via global unfolding should show a one-to-one correlation with ΔG_u°, while those with contributions from native exchange should fall below this limit.

Plots of $-RT \ln(k_{obs}/k_{int})$ versus ΔG_u° for various amino acid residues are presented in Figures 5 and 6. Experimental errors for k_{obs} were propagated through calculations with NonLin. The limited data for Val 4, Val 6, Lys 13, Gly 25, Thr 30, Cys 35, Thr 47, and Leu 50 are not shown, but exchange rates are available as supporting information. A striking result is the general agreement between those experiments with varied pH* at 30 °C (open symbols) and those with varied temperature at pH* 5.5 (filled symbols).

Several interesting trends emerge from the correlation plots (Figures 5 and 6). Exchange for six residues (Leu 23, Ser 26, Asn 28, Asn 33, Val 41, and Ser 51) correlates one-to-one with ΔG_u° (dashed line in Figures 5 and 6). Cys 24, Lys 29, Tyr 31, Cys 35, and Phe 37 may also fall into this group (Figures 5 and 6; class 1, Table 1). This behavior strongly suggests that global unfolding controls hydrogen exchange at these positions. Class 1 sites are not the same as the subset of slowest exchangers, due to variation in k_{int}. In fact, when k_{obs} is ranked at pH* 2.9, exchange rates for class 1 residues Ser 26, Asn 28, and Asn 33 are in the fastest half of the data, while Val 42 (class 2) is much slower. When contributions from intrinsic rates are included, the smallest values of (k_{int}/k_{obs}) still do not equate with class 1: Several of the slowest sites exhibit "superprotection" beyond that predicted by global unfolding, which is discussed in the following paragraphs.

Exchange for a second group of amides appears to have contributions from a process that is unaffected by either temperature or pH. These plots can be described with a model that assumes two competing processes (Qian et al., 1994),

$$-RT \ln\left(\frac{k_{obs}}{k_{int}}\right) = -RT \ln[K_1 + (1 + K_1)K_u] \qquad (4)$$

where K_1 is the equilibrium constant between protected native structure and all exchange-competent native structures of a single residue; this process is assumed to be independent of temperature or pH (Bai et al., 1994; Qian et al., 1994). K_u is the measured global unfolding equilibrium constant that represents conversion of all native states to unfolded protein. Example curves for a series of K_1 values are presented in Figure 7: $-RT$ ln (k_{obs}/k_{int}) plotted as a function of ΔG_u° results in biphasic plots very similar to those of Val 42 and Ser 44 (Figure 6). Plots for Val 4, Val 6, Thr 30, Glu 43, Thr 47, and Cys 56 are also consistent with exchange protection dominated by native fluctuations (Figures 5 and 6; Val 4, Val 6, Thr 30, Thr 47 not shown; class 2, Table 1).

Data for nine other residues also fall below the one-to-one line but continue to show some positive correlation with ΔG_u° where the two-process model indicates that none is expected (Figures 5 and 6; class 3, Table 1). Plots for Tyr 11, Lys 13, Arg 21, Asp 27, Leu 48, Thr 49, His 52, Gly 54, and Lys 55 are described by a continuum of slopes, indicating varying degrees of response to changes in temperature and pH. A surprising fourth class (Table 1) is also evident in Figure 6: Exchange rates for Cys 38, Asn 39, and Ala 40 appear slower than those predicted by the limiting case of global unfolding.

The apparent superprotection can be explained in several ways. However, convergence of exchange rates above 40 °C at pH* 5.0 (supporting information) brings attention to the possibility that the rate of protein refolding (k_2) might be slower than exchange from the exposed site (k_{int}), resulting in EX1 kinetics (Hvidt, 1964; Hvidt & Nielsen, 1966). If so, k_{obs} is controlled solely by the rate at which the site becomes available for exchange (k_1). For behavior intermediate to the EX2 and EX1 limits, exchange is described by the general equation of Hvidt (1964):

$$k_{obs} = \frac{k_1 k_{int}}{k_2 + k_{int}} \qquad (5)$$

Under conditions favoring native protein structure, deviation from pure EX2 kinetics will result in values of $-RT \ln(k_{obs}/k_{int})$ that are larger than ΔG_u°. For example, if k_2 is equal to k_{int}, then the value of $K_{u,app}$ determined by hydrogen exchange is one-half the value of $K_{u,true}$ and $\Delta G_{u,app}^\circ$ is 0.4 kcal/mol larger than $\Delta G_{u,true}^\circ$ (Bai et al., 1994).

One test of EX2 versus EX1 kinetics utilizes the nuclear Overhauser effect (NOE; Wagner, 1980) and has been applied successfully by Roder et al. (1985a), Tüchsen and Woodward (1987), and Bai et al. (1994). This test is based

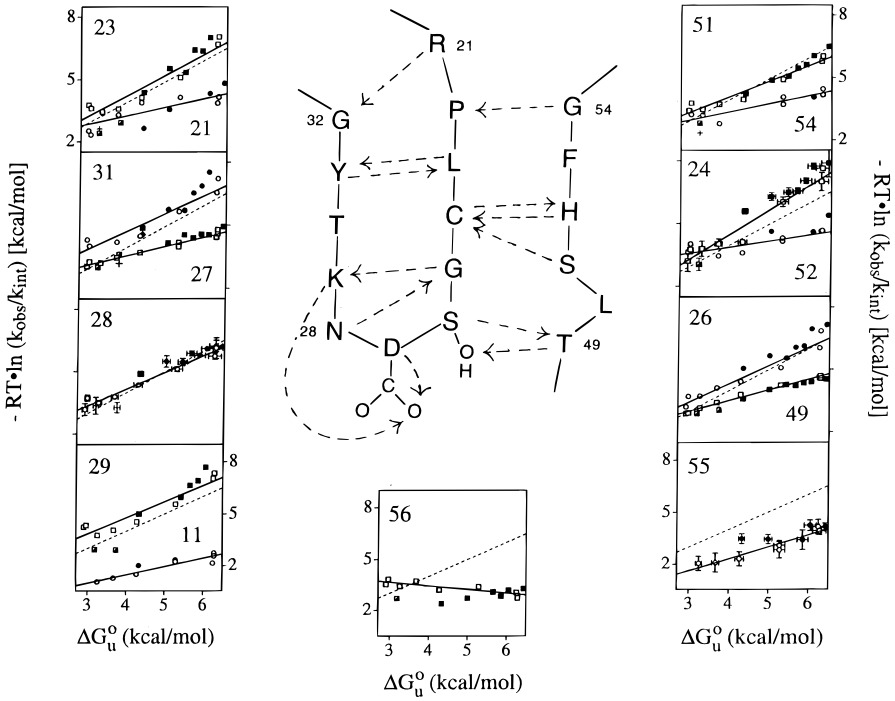

FIGURE 5: Correlation of hydrogen exchange results and the free energy of unfolding for amide hydrogens in the β sheet of OMTKY3. Plots for Tyr 11, Lys 55, and Cys 56 are also included. The quantity $-RT \ln(k_{obs}/k_{int})$ is plotted against ΔG_u° for (□, ○) pH* 1.4, 1.6, 2.1, 2.5, 2.9, 3.5, 4.5, and 5.0 at 30 °C; (■, ●) 27, 34, 37, 40, 43, 48, and 55 °C at pH* 5.0. For experiments at pH* 2.7 and 3.0 at 40°C, the symbol + is used for sites represented by ○ and ●, while ◪ denotes data for a site otherwise described by □ and ■. The dashed line represents the curve $y = x$. The plot for Asn 28 shows data for all possible solution conditions; exchange for some sites could not be determined under all conditions. In some cases, two exchange experiments are reported at pH* 3.5 and 5.0. Representative error bars at one standard deviation are shown on panels for Cys 24, Asn 28, and Lys 55. Solid lines are from linear regression of the pH* data at 30 °C and are presented only to aid visual inspection. Values of ΔG_u° and their errors were calculated according to Swint-Kruse and Robertson (1995). Arrows on the schematic of the β sheet represent hydrogen bonds. When possible, correlation plots for hydrogen-bonded residues are on the same graph.

upon the premise that two sites close in space, A and B, experience the same opening and closing events. In the EX2 limit, A and B will exhibit random exchange relative to each other, and the intensity of the NOE (AB) between these sites, P_{AB}, will be the product of the probabilities that A and B are protonated ($P_A P_B$). Therefore, the decay rate of AB, k_{AB}, will be the sum of the exchange rates for A and B ($k_A + k_B$). Furthermore, if values of k_{int} are different for A and B, k_A and k_B will also be different from each other. However, in the EX1 limit, A and B will exchange at the same instant. Therefore, $P_{AB} = P_A = P_B$ and $k_{AB} = k_A = k_B$.

This test was applied to OMTKY3 hydrogen exchange under the conditions that might favor EX2 kinetics, pH* 3.0 and 40 °C. The intensities of only a few NH/NH NOEs could be measured accurately. Results are presented in Table 2. The quality of the data is affected adversely by low-intensity NOEs, long acquisition times that decrease the number of time points 10-fold relative to an experiment monitored with COSY, and uncertainties introduced by using multiple samples. However, the data suggest EX1 kinetics for at least three sites at pH* 3.0 and 40 °C: Phe 37, Cys 38, and Asn 39. EX2 kinetics can also be tentatively identified at pH* 3.0, 40 °C, since k_A and k_B are different for Ala 40, Val 41, and Val 42. Variations in k_{int} do allow for the possibility of both EX2 and EX1 kinetics under the same experimental conditions. The only previous example of EX1 kinetics under such mild conditions is exchange for HEW lysozyme detected by mass spectrometry (Miranker et al., 1993).

DISCUSSION

The combination of breadth and detail in this experimental design has proven very informative. Exchange rates for more than 30 sites in OMTKY3 have been monitored as a function of protein stability, and several previous observations may be corroborated. First, contributions from the pH dependence of OMTKY3 stability explain shifts in the pH* and rate of slowest exchange, pH_{min} and k_{min}, for most plots of k_{obs} versus pH* (Figure 3), as suggested by Tanford (1970) and Matthew and Richards (1983). Next, most sites showing slowed exchange are involved in hydrogen bonds with coincident solvent exclusion of the amide proton (Figure 4), and one cannot distinguish which of the two physical features is responsible for exchange protection (Lee & Richards, 1971; Chothia, 1976; Wedin et al., 1982; Radford et al., 1992). Furthermore, data from experiments in which pH* and temperature have been employed to change protein stability overlap in the correlation plots (Figures 5 and 6). If exchange experiments indeed monitor structural equilibria, then the exchange competent and incompetent states are independent of the perturbant and are affected to the same extent relative to changes in ΔG_u°.

Across these ranges of temperature and pH*, six to eleven sites show one-to-one correlation with values of ΔG_u° determined from independent thermal denaturation experiments (class 1, Table 1; Figures 5 and 6; Swint-Kruse & Robertson, 1995). This agreement is remarkable, given the differences in intrinsic exchange rates. For example, two conditions where OMTKY3 has similar values of ΔG_u°,

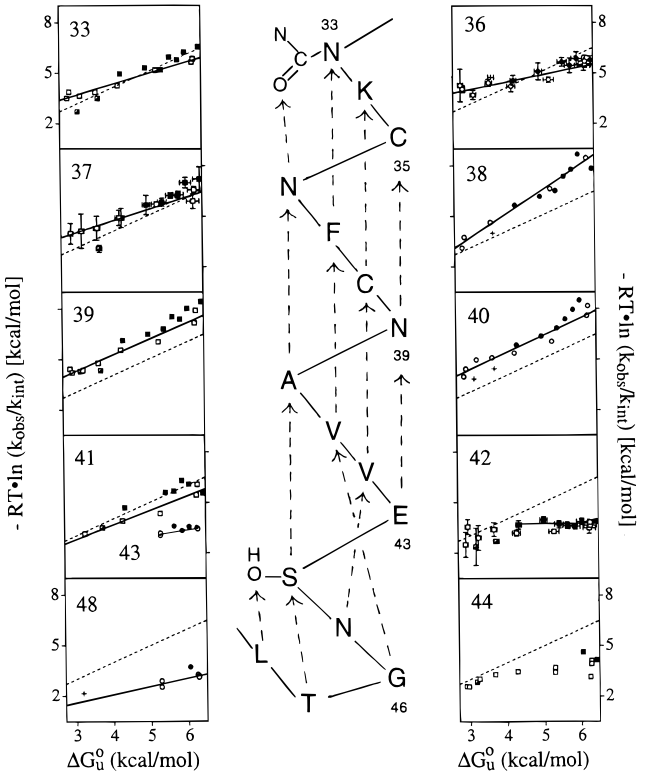

FIGURE 6: Correlation of hydrogen exchange results and the free energy of unfolding for amide hydrogens in and near the α helix of OMTKY3. The quantity $-RT\ \ln(k_{obs}/k_{int})$ is plotted against ΔG°_u for (□, ○) pH* 1.4, 1.6, 2.1, 2.5, 2.9, 3.5, 4.5, and 5.0 at 30 °C; (■, ●) 27, 34, 37, 40, 43, 48, and 55 °C at pH* 5.0. For experiments at pH* 2.7 and 3.0 at 40 °C, the symbol + is used for sites represented by ○ and ●, while ◪ denotes data for a site otherwise described by □ and ■. The dashed line represents the curve $y = x$. The plot for Asn 33 shows data for all possible solution conditions; exchange for some sites could not be determined under all conditions. In some cases, two exchange experiments are reported at pH* 3.5 and 5.0. Representative error bars at one standard deviation are shown on panels for Asn 36, Phe 37, and Val 42. Solid lines are from linear regression of the pH* data at 30 °C and are presented only to aid visual inspection; the exception is Val 42, whose line represents regression of the temperature data. Values of ΔG°_u and their errors were calculated according to Swint-Kruse and Robertson (1995). Arrows on the schematic of the α helix represent hydrogen bonds.

pH* 2.9 at 30 °C and pH* 5.0 at 55 °C, lead to k_{int} values that differ by 3 orders of magnitude. Our conclusion is that exchange at these sites is dominated by global unfolding. These residues do not comprise the same subset as the slowest exchangers or even the smallest values of (k_{obs}/k_{int}), as is commonly assumed. Exchange must be occurring from a denatured structure that is disordered, since residual interactions would further slow exchange. All class 1 residues are part of secondary structure in native OMTKY3, but their side chains are not necessarily part of the hydrophobic core.

Patterns of exchange within OMTKY3 secondary structures are similar to those seen in other proteins (Calhoun & Englander, 1985; Gallagher et al., 1992; Radford et al., 1992; Kim et al., 1993). Generally, residues in the middle of OMTKY3 β strands (23, 24, 28, 29, 31, and 51) are in class 1, while those at the ends (21, 27, 49, and 54) fall into class 3. This pattern is true even when members of different classes are hydrogen bonded to one another, as in the case of Ser 26 and Thr 49 (Figure 5). A group of class 1 residues

Table 1: Hydrogen Exchange Behaviors of Amide Protons in OMTKY3[a]

class 1 one-to-one correlation with ΔG°_u	class 2 two-process exchange[b]	class 3 faster exchange, some correlation with ΔG°_u	class 4 "super-protection"	other
Leu 23	Val 4[c]	Tyr 11	Cys 38	Asn 36[d]
Cys 24[e]	Val 6[c]	Lys 13[c]	Asn 39	Leu 50[c,f]
Ser 26	Thr 30[c]	Arg 21	Ala 40	
Asn 28	Val 42	Asp 27		
Lys 29[e]	Glu 43	Leu 48		
Tyr 31[e]	Ser 44	Thr 49		
Asn 33	Thr 47[c]	His 52		
Cys 35[c]		Gly 54		
Phe 37[e]	Cys 56	Lys 55		
Val 41				
Ser 51				

[a] These tentative classifications are based upon plots of $-RT\ \ln(k_{obs}/k_{int})$ versus ΔG°_u (Figures 5−7). [b] Exchange is consistent with behavior predicted by the two-process model described by eq 4. [c] Only limited exchange data is available and is not shown. [d] See Figure 6. [e] Italics indicate that this residue may belong to class 4. [f] Exchange protection decreases with increased ΔG°_u (data not shown).

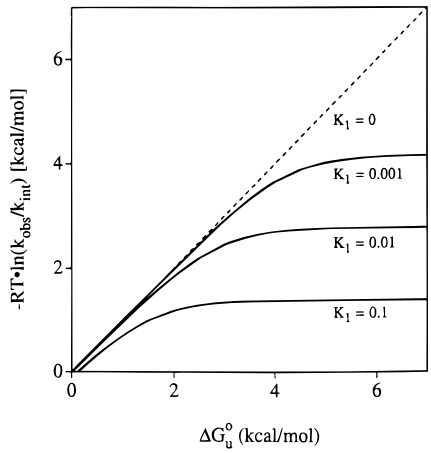

FIGURE 7: Exchange behavior predicted by the two-process model. Equation 4 has been used to generate plots of $-RT\ \ln(k_{obs}/k_{int})$ versus ΔG°_u for a series of K_1 values ranging from 0 (dotted line) to 0.1 (solid curves).

(26, 28, 29, and 51) cluster around the β turn. Subsecondary patterns are also identified in the helix of OMTKY3. Class 1 residues (33, 37, and 41) line the hydrophobic face of the α helix. The N-terminal half (Figure 6) appears to be better protected than the C-terminal half (42−44), which has some 3_{10} characteristics. Interpretation of exchange in the middle of the helix is complicated by deviation from EX2 kinetics and is discussed below.

Exchange from residues in irregular regions of OMTKY3 is generally too fast to measure, even for amides involved in hydrogen bonds (e.g., Asp 7 and Glu 19). Tyr 11, which falls into class 3, is an exception to this rule. Exchange at Tyr 11 may be slowed because its hydrogen bond to Cys 8 is "networked" to the α helix via a disulfide bond with Cys 38. The physical origin for slow exchange at Thr 30, Leu 50, and Lys 55 is a mystery, since these amides are not involved in hydrogen bonds or significantly excluded from solvent (Fujinaga et al., 1987; Krezel et al., 1994; Figure 4). Since exchange for Lys 55 is slowed across a wide pH* range (Figure 5), this phenomenon is probably not due to hydrogen-bonded carbonyl oxygens slowing acid-catalyzed exchange (Tüchsen & Woodward, 1985a,b; Rohl & Baldwin,

Table 2: EX1 versus EX2 Kinetics[a] at pH* 3.0, 40 °C

residue	k_A or k_B	$k_A + k_B$	k_{AB}	HX type[b]
28	16 (7.9)			
		28 (8.0)	16 (4.5)	nd[c]
29	12 (1.2)			
37	6.1 (1.8)			
		10.7 (2.1)	3.4 (2.4)	EX1
38	4.6 (1.1)			
		10.4 (1.3)	4.7 (3.3)	EX1
39	5.8 (0.78)			
		7.0 (0.80)	6.6 (4.3)	EX2
40	1.2 (0.19)			
		1.8 (0.24)	2.9 (0.28)	EX2
41	0.58 (0.14)			
		2.0 (0.20)	2.3 (1.1)	EX2
42	1.4 (0.14)			

[a] Observed rates for peaks A and B, k_A and k_B, represent exchange of NH/CH NOEs. The rates for peaks designated AB, k_{AB}, were determined from the decay of NH/NH NOEs. The units of all rate constants are $s^{-1} \times 10^{-5}$. Numbers in parentheses are fitting errors at 1 σ. [b] EX1 and EX2 are the limiting mechanisms of hydrogen exchange discussed in the text. EX1 kinetics are defined where $k_A = k_B = k_{AB}$, while for EX2 kinetics, $k_{AB} = k_A + k_B$ and often $k_A \neq k_B$. [c] The magnitudes of the fitting errors do not permit assignment of HX type.

1994). Similarly puzzling results were obtained for solvent-exposed Val 39 of staphylococcal nuclease (Loh et al., 1993). Future studies of these residues are warranted, since a complete description of the physical mechanisms leading to slow exchange will only follow from understanding factors responsible for protection observed in exposed residues.

The exchange rates for class 2 residues may be explained by contributions from two competing pathways, global unfolding and native exchange (eq 4, Figure 7). At high protein stability, these sites could exchange by local unfolding events that are independent of temperature and pH* but are overtaken by global unfolding at lower protein stability (Kim & Woodward, 1993; Qian et al., 1994). Val 42 and Ser 44 provide the best examples of this behavior (Figure 6). Their behavior is not explained by a local electrostatic effect of Glu 43 (Matthew & Richards, 1983; Delepierre et al., 1987), as the breakpoint of both curves occurs between pH* 2.9 and 2.5, well below the region where Glu 43 is ionizing (Schaller & Robertson, 1995). The correlation plot for Glu 43 may also be biphasic (Figure 6), but the exchange rates cannot be measured at higher temperatures or be resolved from those of Leu 48 at pH* below 3.5. A final consideration was whether the curves are artifacts of k_{int} calculations, which rely on choosing either the native or denatured pK_a when determining the ionization state of Glu 43. However, the pK_a of Glu 43 in native OMTKY3 is not very different from those of model compounds, which are used to approximate values in denatured protein (Schaller & Robertson, 1995; Swint-Kruse & Robertson, 1995). Furthermore, the value of k_{int} for Val 42 does not contain side chain corrections from Glu 43 (Bai et al., 1993).

The choice of pK_a is more complicated for Asp 27. When the pK_a in native OMTKY3, 2.3, is utilized to calculate k_{int} (Schaller & Robertson, 1995), a biphasic correlation plot is obtained (not shown). This curve cannot be explained by the two - process model: The plot of $-RT \ln(k_{obs}/k_{int})$ appears to be independent of protein stability at low pH* with a switch to class 3 behavior between pH* 3.5 and 4.5. In contrast, exchange data for experiments with varied temperature at pH* 5.0, where Asp 27 is mostly unprotonated in both native and denatured OMTKY3, always fall into class 3. When k_{int} is calculated using the pK_a for denatured OMTKY3 (3.6; P. M. Bowers, A. Walther, and A. D. Robertson, unpublished data; Swint-Kruse & Robertson, 1995), the pH* data are monophasic (Figure 5). Furthermore, changes in pH* and temperature now appear to affect exchange at Asp 27 in the same manner (Figure 5). The choice of pK_a for Asp 27 also affects k_{int} calculations for Asn 28. Correlation plots determined from both pK_as fall into class 1, but pH* and temperature results are in much better agreement when the value of 3.6 is used (plot from native pK_a not shown; denatured pK_a, Figure 5). These observations suggest that the pK_a for Asp 27 in denatured protein is more appropriate.

The only other ionizing residue for which exchange was measured is the C-terminal Cys 56. However, a similar exercise had very little effect on the data: Changing the pK_a of the C terminus from the native value of 2.4 to 3.1, the estimated value for denatured protein (Schaller & Robertson, 1995; Swint-Kruse & Robertson, 1995), affects $-RT \ln(k_{obs}/k_{int})$ by less than 0.05 kcal/mol.

A few features of the data are not immediately explained by the two-process model. Class 3 behavior is a conspicuous example. These sites exchange faster than the limit predicted by global unfolding but are affected by perturbations of stability. Their plots are not explained by models including either an unfolding intermediate or deviation from EX2 kinetics for global unfolding in derivations of eq 4. One hypothesis is these sites undergo native fluctuations that are also sensitive to changes in pH* and temperature. Bai et al. (1995) have postulated that similar behavior observed for cytochrome *c* reflects exchange from partially unfolded structures.

An additional inconsistency with the two-process model is the low pH* "tail" observed in correlation plots for residues 23, 27, 29, 31, 33, 36, 37, 51, 52, and 56 (Figures 5 and 6). In these plots, data at pH* 1.4 and 1.6 (the two leftmost points) consistently deviate from the other data and are often above the one-to-one line. This deviation is most likely a result of low pH* and not of decreased protein stability, since experiments at pH* 2.7 and 3.0 at 40 °C are consistent with all other data (Figures 5 and 6, ◪ and +). At least four scenarios could give rise to this behavior: (1) deviation from EX2 kinetics (Bai et al., 1994), (2) exchange from an acid intermediate with a higher free energy than the unfolded state, (3) high local concentrations of OH^- affecting values of k_{int} (Kim & Baldwin, 1982); and (4) hydrogen bonds at carbonyl oxygens slowing acid-catalyzed exchange (Tüchsen & Woodward, 1985a,b; Rohl & Baldwin, 1994). We suspect the latter possibility, although no evidence is currently available for distinguishing between the four.

Another prominent feature of the OMTKY3 data that is not explained by the two-process model is the apparent superprotection of class 4 sites (Figure 6, Table 1). Similar results have been obtained for Cys 58 in RNase A (Mayo & Baldwin, 1993), Ala 96 and Tyr 97 of equine cytochrome *c* (Bai et al., 1994), Asp 52 and Cys 64 of HEW lysozyme (Radford et al., 1992), and seven residues in yeast iso-1-cytochrome c (Marmorino et al., 1993). In OMTKY3, this phenomenon is not due to differences in solution conditions, as has been previously suggested for other proteins (Bai et al., 1994; Qian et al., 1994), nor is this behavior likely to be

due to innaccurate k_{int} values: the dipeptide sequence Cys-Asn occurs twice in OMTKY3, at residues 35/36 and 38/39, but the Asn correlation plots are very different (Figure 6). At least three other circumstances could lead to superprotection: (1) exchange from an intermediate with a free energy larger than the denatured state's (Marmorino et al., 1993; Bai et al., 1994), (2) a shift in the ensemble of denatured states from that of the high-temperature denatured state (Dill & Shortle, 1991; Wang et al., 1995), and (3) deviation from EX2 kinetics (Marmorino et al., 1993; Bai et al., 1994). Evidence for the latter possibility comes from comparison of k_{obs} at temperatures $\geq$40 °C and from monitoring the decay of NH/NH NOEs (Table 2; Wagner, 1980). Moreover, inspection of the correlation plots shows that, in some instances, data at pH* 5.0, 55 °C (usually the leftmost solid symbol) deviates from the rest of the data, suggesting the possibility of widespread EX1 behavior at pH* 5 and 55 °C.

EX1 kinetics occur when $k_{int} \gg k_2$, the rate of protein folding. The kinetics of OMTKY3 folding have not been measured, but the exchange data suggest that at pH* 5.0 and 55 °C, k_2 may be slower than k_{int} for Cys 38, which is 0.5 s^{-1}. Slow folding around Cys 38 presents the intriguing possibility of slow isomerization for loops constrained by disulfide bonds (Nall et al., 1978). Extreme protection has also been seen for disulfide-bonded cysteines in HEW lysozyme (Radford et al., 1992) and RNase A (Mayo & Baldwin, 1993), which suggests this may be a more general phenomenon. Pedersen et al. (1993) similarly proposed slow closing reactions for residues located in the middle of helices in HEW lysozyme. Deviation from EX2 kinetics has been directly observed with electrospray ionization mass spectrometry for HEW lysozyme hydrogen exchange at pH 3.8, 69 °C (Miranker et al., 1993). EX1 exchange has also been inferred from anamolous pH dependences of exchange for HEW lysozyme at pH > 6 and 21 °C (Pedersen et al., 1993) and barnase at pH > 6.7 and 37 °C (Perrett et al., 1995). Taken together, these results suggest that EX2 kinetics should not be assumed in interpretation of hydrogen exchange experiments.

This study demonstrates that global unfolding dominates exchange at some sites in OMTKY3 and that exchange rates contain quantitative information about structural equilibria. Nearly one-third of the residues monitored show one-to-one correlation with ΔG°_{u} at temperatures very far from those of the unfolding transition. These sites are not the slowest exchangers or those exhibiting greatest protection. Exchange at some other sites is consistent with a simple two-process model, but neither two-process nor global unfolding explains exchange for more than one-third of the amides. Finally, changes in pH* and temperature affect exchange data in the same manner, indicating that the same structural equilibria are affected by the two perturbants.

ACKNOWLEDGMENT

We thank Dr. William R. Kearney for his invaluable help running the NMR spectrometer and Dr. Kenneth P. Murphy for many insightful discussions. Drs. D. W. Bolen, S. W. Englander, J. Martin Scholtz, and Charles A. Swenson contributed helpful comments on the manuscript. Theis Farms generously donated many turkey eggs.

SUPPORTING INFORMATION AVAILABLE

Observed exchange rates (k_{obs}) for all sites measured are available in three tables: data for pH* 1.4 to 5.0 at 30 °C (Table 1); data for pH* 5.0, 27−55 °C (Table 2); and rates measured at pH* 2.7 and 3.0 at 40 °C (Table 3) (8 pages). Ordering information is given on any current masthead page.

REFERENCES

Antosiewicz, J., McCammon, J. A., & Gilson, M. K. (1994) *J. Mol. Biol. 238,* 415−436.
Arcus, V. L., Vuilleumier, S., Freund, S. M. V., Bycroft, M., & Fersht, A. R. (1994) *Proc. Natl. Acad. Sci. U.S.A. 91,* 9412−9416.
Aue, W. P., Bartholdi, E., & Ernst, R. R. (1976) *J. Chem. Phys. 64,* 2229−2246.
Bai, Y., Milne, J. S., Mayne, L., & Englander, S. W. (1993) *Proteins 17,* 75−86.
Bai, Y., Milne, J. S., Mayne, L., & Englander, S. W. (1994) *Proteins 20,* 4−14.
Bai, Y., Sosnick, T. R., Mayne, L., & Englander, S. W. (1995) *Science 269,* 192−197.
Barksdale, A. D., & Rosenberg, A. (1982) *Methods Biochem. Anal. 28,* 1−113.
Bode, W., Epp, O., Huber, R., Laskowski, M. Jr., & Ardelt, W. (1985) *Eur. J. Biochem. 147,* 387−395.
Brenstein, R. J. *NonLin for the Macintosh,* Robelko Software, Carbondale, IL.
Buck M., Radford, S. E., & Dobson, C. M. (1992) *Biochemistry 237,* 247−254.
Calhoun, D. B., & Englander, S. W. (1985) *Biochemistry 24,* 2095−2100.
Chothia, C. (1976) *J. Mol. Biol. 105,* 1−14.
Clarke, J., Hounslow, A. M., Bycroft, M., & Fersht, A. R. (1993) *Proc. Natl. Acad. Sci. U.S.A. 90,* 9837−9841.
Connelly, P. R., Thomson, J. A., Fitzgibbon, M. J., & Bruzzese, F. J. (1993) *Biochemistry 32,* 5583−5590.
Delepierre, M., Dobson, C. M., Karplus, M., Poulsen, F. M., States, D. J., & Wedin, R. E. (1987) *J. Mol. Biol. 197,* 111−130.
Dill, K. A., & Shortle, D. (1991) *Annu. Rev. Biochem. 60,* 795−825.
Englander, S. W., Calhoun, D. B., Englander, J. J., Kallenbach, R. K., Liem. H., Malin, E. L., Mandal, C., & Rogero, J. R. (1980) *Biophys J. 32,* 577−591.
Englander, S. W., & Kallenbach, N. R. (1984) *Q. Rev. Biophys. 16,* 521−655.
Fujinaga, M., Sielecki, A., Read., R. J., Ardelt, W., Laskowski, M., Jr., & James, M. N. G. (1987) *J. Mol. Biol. 195,* 397−418.
Gallagher, W., Tao, F., & Woodward, C. (1992) *Biochemistry 31,* 4673−4680.
Hermans, J., Jr., & Scheraga, H. A. (1959) *Biochim. Biophys. Acta 36,* 534−535.
Horovitz, A., Serrano, L., Avron, B., Bycroft, M., & Fersht, A. R. (1990) *J. Mol. Biol. 216,* 1031−1044.
Hvidt, A. (1964) *C. R. Trav. Lab. Carlsberg 34,* 299−317.
Hvidt, A., & Nielsen, S. O. (1966) *Adv. Protein Chem. 21,* 287−386.
Jandu, S. K., Ray, S., Brooks, L., & Leatherbarrow, R. J. (1990) *Biochemistry 29,* 6264−6269.
Jencks, W. P. (1969) *Catalysis in Chemistry and Enzymology,* McGraw-Hill, New York.
Johnson, M. L., & Frasier, S. G. (1985). *Methods Enzymol. 117,* 301−342.
Johnson, M. L., & Faunt, L. M. (1992). *Methods Enzymol. 210,* 1−37.
Kim, K. S., & Woodward, C. K. (1993) *Biochemistry 32,* 9609−9613.
Kim, K. S., Fuchs, J. A., & Woodward, C. K. (1993) *Biochemistry 32,* 9600−9608.
Kim, P. S., & Baldwin, R. L. (1982) *Biochemistry 21,* 1−5.
Krezel, A. M., Darba, P., Robertson, A. D., Fejzo, J., Macura, S., & Markley, J. L. (1994) *J. Mol. Biol. 242,* 203−214.
Kumar, A., Ernst, R. R., & Wüthrich, K. (1980) *Biochem. Biophys. Res. Commun. 95,* 1−6.

Laskowski, M., Jr., Kato, I., Ardelt, W., Cook, J., Denton, A., Empie, M. W., Kohr, W. J., Park, S. J., Parks, K., Schatzley, B. L., Schoenberger, O. L., Tashiro, M., Vichot, G., Whatley, H. E., Wieczorek, A., & Wieczorek, M. (1987) *Biochemistry 26*, 202−221.
Lee, B. K., & Richards, F. M. (1971) *J. Mol. Biol. 55*, 379−400.
Lemm, U., & Wenzel, M. (1981) *Eur. J. Biochem. 116*, 441−445.
Linderstrøm-Lang, K. (1955) *Spec. Publ. Chem. Soc. 2*, 1−20.
Loh, S. N., Prehoda, K. E., Wang, J., & Markley, J. L. (1993) *Biochemistry 32*, 11022−11028.
Lu, J., & Dahlquist, F. W. (1992) *Biochemistry 31*, 4749−4756.
Marmorino, J. L., Auld, D. S., Betz, S. F., Doyle, D. F., Young, G. B., & Pielak, G. J. (1993) *Protein Sci. 2*, 1966−1974.
Matthew, J. B., & Richards, F. M. (1983) *J. Biol. Chem. 258*, 3039−3044.
Mayo, S. L., & Baldwin, R. L. (1993) *Science 262*, 873−876.
Miranker, A., Robinson, C. V., Radford, S. E., Aplin, R. T., & Dobson, C. M. (1993) *Science 262*, 896−900.
Molday, R. S., Englander, S. W., & Kallen, R. G. (1972) *Biochemistry 11*, 150−158.
Nall, B. T., Garel, J. R., & Baldwin, R. L. (1978) *J. Mol. Biol. 118*, 317−330.
Pedersen, T. G., Thomsen, N. K., Andersen, K. V., Madsen, J. C., & Poulsen, F. M. (1993) *J. Mol. Biol. 230*, 651−660.
Perrett, S., Clarke, J., Hounslow, A. M., & Fersht, A. R. (1995) *Biochemistry 34*, 9288−9298.
Qian, H., Mayo, S. L., & Morton, A. (1994) *Biochemistry 33*, 8167−8171.
Radford, S. E., Buck, M., Topping, K. D., Dobson, C. M., & Evans, P. A. (1992) *Proteins: Struct. Funct. Genet. 14*, 237−248.
Robertson, A. D. (1988) Ph.D. Thesis, University of Wisconsin, Madison, WI.
Robertson, A. D., & Baldwin, R. L. (1991) *Biochemistry 30*, 9907−9914.
Robertson, A. D., Westler, W. M., & Markley, J. L. (1988) *Biochemistry 27*, 2519−2529.
Roder, H. (1989) *Methods Enzymol. 176*, 446−473.
Roder, H., Wagner, G., & Wüthrich, K. (1985a) *Biochemistry 24*, 7396−7407.
Roder, H., Wagner, G., & Wüthrich, K. (1985b) *Biochemistry 24*, 7407−7411.
Rohl, C. A., & Baldwin, R. L. (1994) *Biochemistry 33*, 7760−7767.
Rosenberg, A., & Chakravarti, K. (1968) *J. Biol. Chem. 243*, 5193−5201.
Šali, D., Bycroft, M., & Fersht, A. R. (1991) *J. Mol. Biol. 220*, 779−788.
Schaller, W. A., & Robertson, A. D. (1995) *Biochemistry 34*, 4714−4723.
Scholtz, J. M., & Robertson, A. D. (1995) In *Methods in Molecular Biology, Vol. 40: Protein Stability and Folding, Theory and Practice* (Shirley, B. A., Ed.): pp 291−311, Humana Press, Inc., Totowa, NJ.
Shalongo, W., Dugad, L., & Stellwagen, E. (1994) *J. Am. Chem. Soc. 116*, 8288−8293.
Stigter, D., & Dill, K. A. (1990) *Biochemistry 29*, 1262−1271.
Swint, L., & Robertson, A. D. (1993) *Protein Sci. 2*, 2037−2049.
Swint-Kruse, L., & Robertson, A. D. (1995) *Biochemistry 34*, 4724−4732.
Tanford, C. (1970) *Adv. Protein Chem. 24*, 1−95.
Tüchsen, E., & Woodward, C. (1985a) *J. Mol. Biol. 185*, 405−419.
Tüchsen, E., & Woodward, C. (1985b) *J. Mol. Biol. 185*, 421−430.
Tüchsen, E., & Woodward, C. (1987) *Biochemistry 26*, 8073−8078.
Van Geet, A. L. (1968) *Anal. Chem. 40*, 2227−2229.
Wagner, G. (1980) *Biochem. Biophys. Res. Commun. 97*, 614−620.
Wagner, G., & Wüthrich, K. (1979) *J. Mol. Biol. 134*, 75−94.
Wagner, G., & Wüthrich, K. (1982) *J. Mol. Biol. 160*, 343−361.
Wang, A.-J., Robertson, A. D., & Bolen, D. W. (1995) *Biochemistry 34*, 15096−15104.
Wedin, R. E., Delepierre, M., Dobson, C. M., & Poulsen, F. (1982) *Biochemistry 21*, 1098−1103.
Woodward, C. K., & Hilton, B. D. (1979) *Ann. Rev. Biophys. Bioeng. 8*, 99−127.
Woodward, C. K., & Hilton, B. D. (1980) *Biophys. J. 32*, 561−577.
Wüthrich. K., Wagner, G., Richarz. R., & Braun, W. (1980) *Biophys. J. 32*, 549−561.

BI9517603